Research Square

Preprints are preliminary reports that have not undergone peer review.
They should not be considered conclusive, used to inform clinical practice,
or referenced by the media as validated information.

Mapping Mediterranean marginal lands as opportunity spaces for climate-resilient agrifood diversification

Luigi Tosi

luigi.tosi@cnr.it

National Research Council https://orcid.org/0000-0001-5254-4059

Cristina Da Lio

National Research Council

Marta Cosma

Institute of Geosciences

Taoufik Hermassi

2National Research Institute of Rural Engineering, Water and Forests, Laboratory of Rural Engineering

Mohamed Lassaad Kotti

National Research Institute of Rural Engineering, Water and Forests, Laboratory of Rural Engineering

Fathia Jarray

National Research Institute of Rural Engineering, Water and Forests, Laboratory of Rural Engineering

Vassilis Aschonitis

Hellenic Agricultural Organization-DIMITRA, Soil and Water Resources Institute

Sandra Donnici

National Research Council

Article

Keywords: Mediterranean marginal lands, Climate-resilient agriculture, Neglected and Underutilized Species, Agroecological opportunity spaces, Climate adaptation strategies

Posted Date: July 21st, 2026

DOI: https://doi.org/10.21203/rs.3.rs-10336127/v1

License: This work is licensed under a Creative Commons Attribution 4.0 International License.
Read Full License

Additional Declarations: There is **NO** Competing Interest.

Mapping Mediterranean marginal lands as opportunity spaces for climate-resilient agrifood diversification

Luigi Tosi[1]*, Cristina Da Lio[1]*, Marta Cosma[1], Taoufik Hermassi[2], Mohamed Lassaad Kotti[2], Fathia Jarray[2], Vassilis Aschonitis[3], Sandra Donnici[1]

[1]National Research Council of Italy, Institute of Geosciences, Padova, Italy
[2]National Research Institute of Rural Engineering, Water and Forests, Laboratory of Rural Engineering, Ariana, Tunisia
[3]Hellenic Agricultural Organization-DIMITRA, Soil and Water Resources Institute, Thessaloniki, Greece

Abstract

The Mediterranean region faces escalating challenges from climate change, land degradation, and water scarcity, threatening agricultural sustainability and food security. Stress-adapted Neglected and Underutilized Species (NUS) offer promising avenues for agrifood diversification and resilience in these environments. Here, we developed a harmonized geospatial framework integrating over 20 abiotic indicators and CMIP6 climate projections to delineate environmental constraints and agroecological opportunity spaces across the Mediterranean Basin. Our analysis identified 1.83 million km² of accessible marginal lands, predominantly in climatically sensitive transition zones, with modest expansion projected under future climate scenarios. These marginal lands, rather than being abandoned, represent potential areas for developing stress-adapted diversification strategies. This reproducible dataset provides a decision-oriented basis for climate adaptation, land-use planning, and the strategic assessment of NUS deployment, contributing to resilient agrifood transitions under increasing climatic constraints.

Keywords

Mediterranean marginal lands, Climate-resilient agriculture, Neglected and Underutilized Species, Agroecological opportunity spaces, Climate adaptation strategies.

Main

The Mediterranean basin is experiencing increasing pressure from climate change and human activities, such as population growth, agricultural intensification, and desertification. These factors are causing progressive losses of productive land and declining yields [1,2]. As a recognized climate-change hotspot, the region faces accelerating warming, more frequent droughts, and sea-level rise, all of which intensify structural pressures on land and water resources and threaten food security and ecosystem services. These trends highlight the urgent need for scalable strategies to enhance resilience and reverse land degradation, thereby reducing the risks of water-related conflict, socio-economic instability, and rural impoverishment [1,2].

Water scarcity is increasingly constraining Mediterranean agricultural systems. Declining rainfall, rising evaporative demand, and soil degradation, especially in rainfed systems and coastal plains affected by salinization and saltwater intrusion, are reducing water availability. The combined effects of limited freshwater, salinity stress, and degraded soil are major constraints on agroecosystem functioning and are narrowing viable management options.

At the same time, the Mediterranean basin remains a global biodiversity hotspot [3], hosting plant communities adapted to chronic water limitation, nutrient-poor substrates, and salinity. Many of these taxa are embedded in traditional food systems and constitute a valuable source of bioactive compounds for nutritional, cosmetic, and medicinal applications [4,5]. NUS are plant species that have traditionally received limited attention in research and agricultural development, but are often more resilient than conventional crops. These species offer potential for diversification and sustainable land use under environmental stress [6].

Recent works highlight salt-tolerant and drought-resistant NUS as viable solutions for climate adaptation, serving as alternative crops, components of rotations or intercropping systems, and nature-based tools for soil rehabilitation [7,8]. Examples include emerging applications of salt- and drought-tolerant NUS across Mediterranean systems, from coastal halophytes to dryland crops [9–11]. However, these applications remain largely localized, and broader transferability is limited by strong spatial heterogeneity in climate, soils, and topography, underscoring the need for Mediterranean-wide assessments of abiotic constraints.

To address this gap, we developed a harmonized, Mediterranean-wide geospatial framework (Supplementary Fig. 1) that combines core abiotic soil properties, vegetation, topography, and climate constraints, including CMIP6 projections to 2050 under Shared Socio-economic Pathways (SSP2–4.5 and SSP5–8.5) (Supplementary Note 1). In this study, land marginality is defined not as land

abandonment or intrinsic unsuitability, but as the cumulative expression of environmental constraints that limit the effectiveness of conventional agriculture. By coupling literature-informed thresholds with data-driven climatic clustering, we delineate basin-scale zonation patterns that reveal environmental constraints and agroecological opportunity spaces in which diversification strategies involving stress-adapted NUS can be explored under current and future climatic conditions.

Results

Abiotic stress gradients across the Mediterranean Basin

The pH map shows that most of the basin is dominated by neutral-to-moderately alkaline soil classes (**Fig. 1** and Supplementary Table 1). Higher alkalinity is concentrated in North Africa, particularly in southern Algeria and southwestern Libya, within the central Saharan belt surrounding the Hoggar Mountains (Supplementary Fig. 1). Conversely, acidic soils are mainly found in humid and mountainous regions, such as the Atlas Mountains, northwestern Iberia (Galicia and northern Portugal), northern European mountain systems, and localized areas of the Middle East, including the Pontic Mountains, the southern Black Sea coastal belt of Türkiye, and parts of the Levant highlands.

The salinity map (**Fig. 1** and Supplementary Table 1) highlights spatially discrete yet ecologically significant hotspots, particularly across low-lying coastal plains, arid inland depressions and deltaic systems such as the Nile Delta, the Ebro Delta, the Po Plain, the Gulf of Gabes coastal plain, and the Chott El Jerid basin of Tunisia, where intense evaporation and shallow groundwater interactions promote salt accumulation, often enhanced by saltwater intrusion. Additional saline areas are observed in geomorphologically confined zones with strong evaporative concentration, influenced by shallow groundwater in parts of the Atlas and Levant regions, including the Sousse Plain, the Moulouya Basin, the Jordan Rift Valley, and the Dead Sea Depression.

SOC classes (**Fig. 1** and Supplementary Table 1) reveal a marked north–south gradient, with higher carbon contents concentrated in the northern Mediterranean and mountainous belts, including the Alps, Apennines, Pyrenees, Dinaric Alps, and Balkan Mountains. Lower SOC classes progressively dominate the semi-arid regions of eastern Libya, northern Egypt, the Sinai Peninsula, the Negev Desert, and the Jordan Rift Valley. The statistical distributions (**Fig. 1**) confirm that low-to-moderate SOC classes represent a substantial proportion of the basin, underscoring widespread intrinsic fertility limitations.

Bulk density (**Fig. 1** and Supplementary Table 1) is dominated by low-to-moderate classes across most of the Mediterranean basin. Higher-density classes are concentrated in parts of northeastern

Africa and the Levant, including northern-central Tunisia, the Sinai Peninsula, the Jordan Rift Valley, the Bekaa Valley, and the Lebanon Mountains, with additional hotspots occurring near the foothills of the High Atlas and Carpathian Mountain systems.

The spatial distribution of high-density classes corresponds to environments where low organic carbon content and unfavorable soil physical properties contribute to increased compaction and reduced structural stability. Naturally coarse-textured soils with low organic matter are more susceptible to structural degradation, and mechanical disturbance or grazing pressure can further increase soil density. These interaction factors may lead to compound physical constraints, such as decreased aggregate stability, limited porosity, and impaired water infiltration.

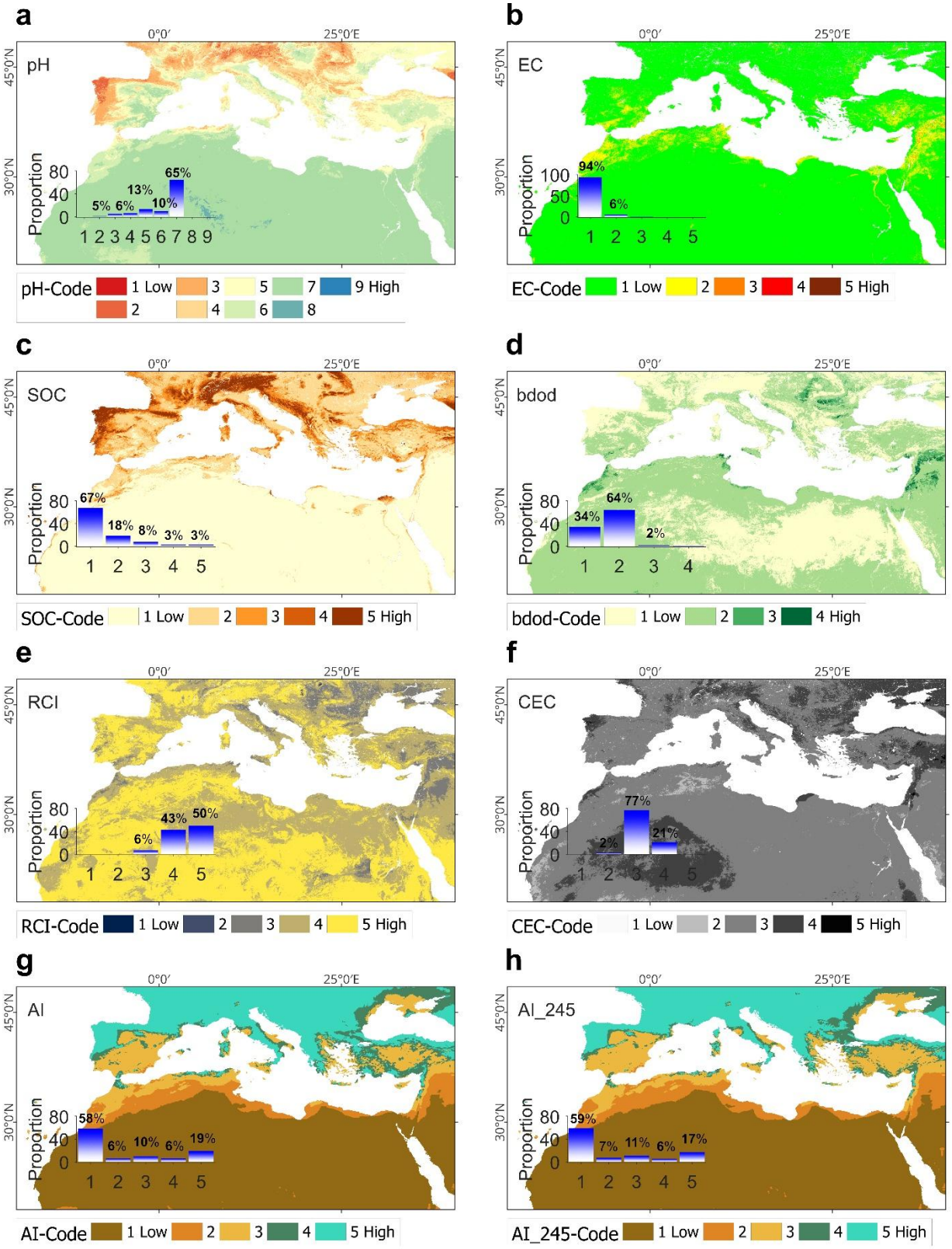
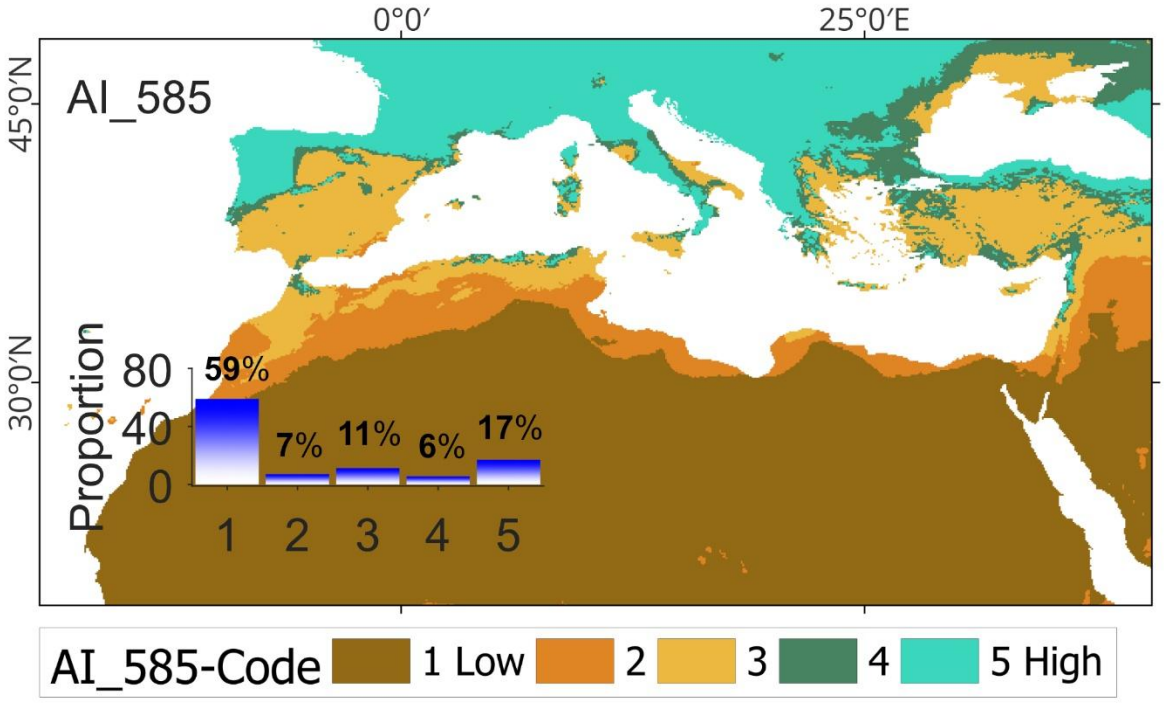


Fig. 1. Mediterranean-wide environmental zonation of abiotic environmental soil parameters based on literature-informed classification. a-d *Classification of core soil stressors and properties:* ***a****, soil acidity (pH);* ***b****, soil salinity (EC),* ***c****, soil organic carbon (SOC),* ***d****, soil bulk density (bdod).* ***e-***

f *Classification of intrinsic productivity indicators:* ***e****, retention curve index (RCI),* ***f****, soil cation exchange capacity (CEC),* ***g****, aridity index (AI),* ***h****, future aridity index under SSP2–4.5 (AI_245) for 2041–2060. Classification code ranges are provided in Supplementary Table 1 and Supplementary Table 2. Bar charts show the proportions of area within each class.*



Extended Data Fig. 1. Mediterranean-wide environmental zonation of the future aridity index under SSP5–8.5 (AI_585) for 2041–2060*. Classification code ranges are provided in Supplementary Table 2. Bar charts show the proportion of area within each class.*

The RCI map (**Fig. 1** and Supplementary Table 2) reveals a heterogeneous mosaic of soil physical quality, with intermediate-to-high classes forming transitional belts in southern Europe, including the Ebro Basin, Po Plain margins, and Pannonian Basin, as well as the Anatolian Plateau, Upper Mesopotamian plains, Tell Atlas foothills, northern Tunisia, the Cyrenaica Plateau, and the Nile Delta. Very high classes occur across the hyper-arid Sahara, including the Tanezrouft Basin, Libyan Desert, and Western Desert of Egypt, as well as semi-arid Iberia (Meseta Central and Ebro Depression), northern European mountain systems (Alps and Carpathians), and several inland basins of the Balkan region, including the Vardar Basin and Morava Valley.

However, the very high RCI observed in hyper-arid regions should not be taken as a sign of readily available plant water. These values mainly indicate good physical soil quality related to texture-specifically, an optimal clay content of about 20%, while the severe water deficit fully suppresses the

agronomic expression of this potential. Accordingly, high RCI values in hyper-arid regions such as the Tanezrouft Basin, the Libyan Desert, and the Western Desert of Egypt must be interpreted with caution. Although they reflect favorable texture-related physical properties, they do not necessarily translate into improved soil functionality under severe water limitation. This underscores the need to interpret each indicator within a broader context, considering how climate limitations can overshadow positive soil traits.

CEC patterns (**Fig. 1** and Supplementary Table 2) broadly mirror texture-related fertility gradients, with higher exchange capacities observed in the Po Plain, Danube Lowlands, Aquitaine Basin, Jordan Rift Valley, Bekaa Valley, Cyrenaica Plateau, Negev Desert, and parts of the Sahara's erg systems. High CEC values also occur in sandy loam soils of the central Sahara surrounding the Hoggar Mountains and across northwestern Iberia, particularly in Galicia and northern Portugal. Most of the basin falls within the moderate CEC class, indicating an intermediate capacity for nutrient retention across Mediterranean agroecosystems. Moderately low CEC classes are concentrated in northeastern Africa, notably the Nile hinterland and the Eastern Desert of Egypt, and in northwestern Africa along the Sahel-Atlas margins and the Maghreb interior plains.

The baseline AI map (**Fig. 1** and Supplementary Table 2) shows a sharp climatic transition from the humid and sub-humid northern Mediterranean, including northern Spain, southern France, northern Italy, Slovenia, and the western Balkans, to the arid southern sectors of the basin, notably the Maghreb interior plains, Chott el Jerid basin, Cyrenaica Plateau, Libyan Desert margin, Jordan Rift Valley, and Syrian Steppe. A broad semi-arid to arid transition belt extends across the central and southern Iberian Peninsula, North Africa, and parts of the Balkans and Middle East, encompassing the Meseta Central, Andalusia, Murcia, the High Plateaus of Algeria, the Sahel Atlas margins, the Thessaly Plain, Central Anatolia, and the Upper Mesopotamian Plain. This transitional belt emerges as a critical zone of climatic sensitivity. Under SSP2–4.5, and SSP5–8.5, arid and semi-arid classes expand modestly poleward, with contraction of sub-humid and humid classes and systematic intensification of aridity in transitional zones by signaling basin-wide amplification of climatic stress rather than isolated shifts (Extended Data Fig. 1). The projected shifts are directionally consistent across scenarios but remain moderate in magnitude. Changes are concentrated in transitional belts, and statistical distributions indicate only a limited redistribution toward lower AI classes under SSP2–4.5 and SSP5–8.5, rather than widespread regime shifts (**Fig. 1**, Extended Data Fig. 1).

Texture classes show extensive sandy-loam and sandy-clay-loam domains across much of the Sahara, including the Grand Erg Occidental, Grand Erg Oriental, Libyan Desert, and Western Desert of Egypt (**Fig. 2** and Supplementary Table 3). These textured areas coincide spatially with hyper-arid to arid

climatic zones, suggesting a potential amplification of drought stress. Conversely, Mediterranean coastal and sub-coastal regions are dominated by loam and clay-loam textures, notably across the Tell Atlas foothills, Cyrenaica Plateau, Nile Delta, Sinai Peninsula, Thessaly Plain, Vardar Basin, much of Italy, the Lower Rhône Valley, Ebro Delta, Segura Basin, Murgia, and Guadalquivir Valley, conditions generally more favorable for agriculture.

Coarse fragments are predominantly concentrated in mountainous and peri-mountainous regions, including the Atlas Mountains, Rif Mountains, Alps, Apennines, Pyrenees, and Taurus Mountains, largely overlapping with steeply sloping terrain (**Fig. 2** and Supplementary Table 3).

Low to moderate coarse-fragment content also characterizes most of the Sahara region, likely linked to widespread, extreme environmental conditions, with high coarse-fragment content detected in the Hoggar Mountains and the Eastern Desert of Egypt due to local resistant bedrock, steep slopes, and weathering.

Topographic maps (elevation and slope, **Fig. 2** and Supplementary Table 3) confirm the presence of steep terrain across major Mediterranean mountain systems, including the Atlas Mountains, Alps, Apennines, Pyrenees, Dinaric Alps, Balkan Mountains, and Taurus Mountains, forming extensive belts of topographic constraint throughout the basin (**Fig. 2** and Supplementary Table 3).

Summer-average NDVI delineates vegetation productivity patterns and identifies marginal or degraded areas characterized by sparse vegetation cover or bare land (**Fig. 2** and Supplementary Table 3). Broad low-productivity zones occur across the arid drylands of North Africa and the Middle East, extending from the Tanezrouft Basin and Libyan Desert to the Sinai Peninsula, Negev Desert, and Syrian Desert. Their spatial correspondence with low SOC and AI classes highlights the close association between climatic aridity and reduced vegetative cover (**Fig. 1** and Supplementary Table 1 and Supplementary Table 2, respectively). The spatial correspondence between summer NDVI and SOC is only partial, as NDVI reflects short-term vegetation activity, whereas SOC represents a long-term soil property shaped by land use, mineralogy, and organic matter inputs.

Land-cover patterns indicate that sparse vegetation and shrub-dominated areas are frequently associated with moderate-to-high abiotic stress classes, particularly in semi-arid transition zones such as the High Plateaus of Algeria, the Chott el Jerid basin, the Ebro Depression margins, the Anatolian Plateau, and the Thessaly Plain. Mediterranean-wide screening was based on the 2014 land-cover dataset (**Fig. 2** and Supplementary Table 3), whereas finer-scale marginal-land assessments used the 2022 dataset (Extended Data **Fig. 2** and Supplementary Table 4).

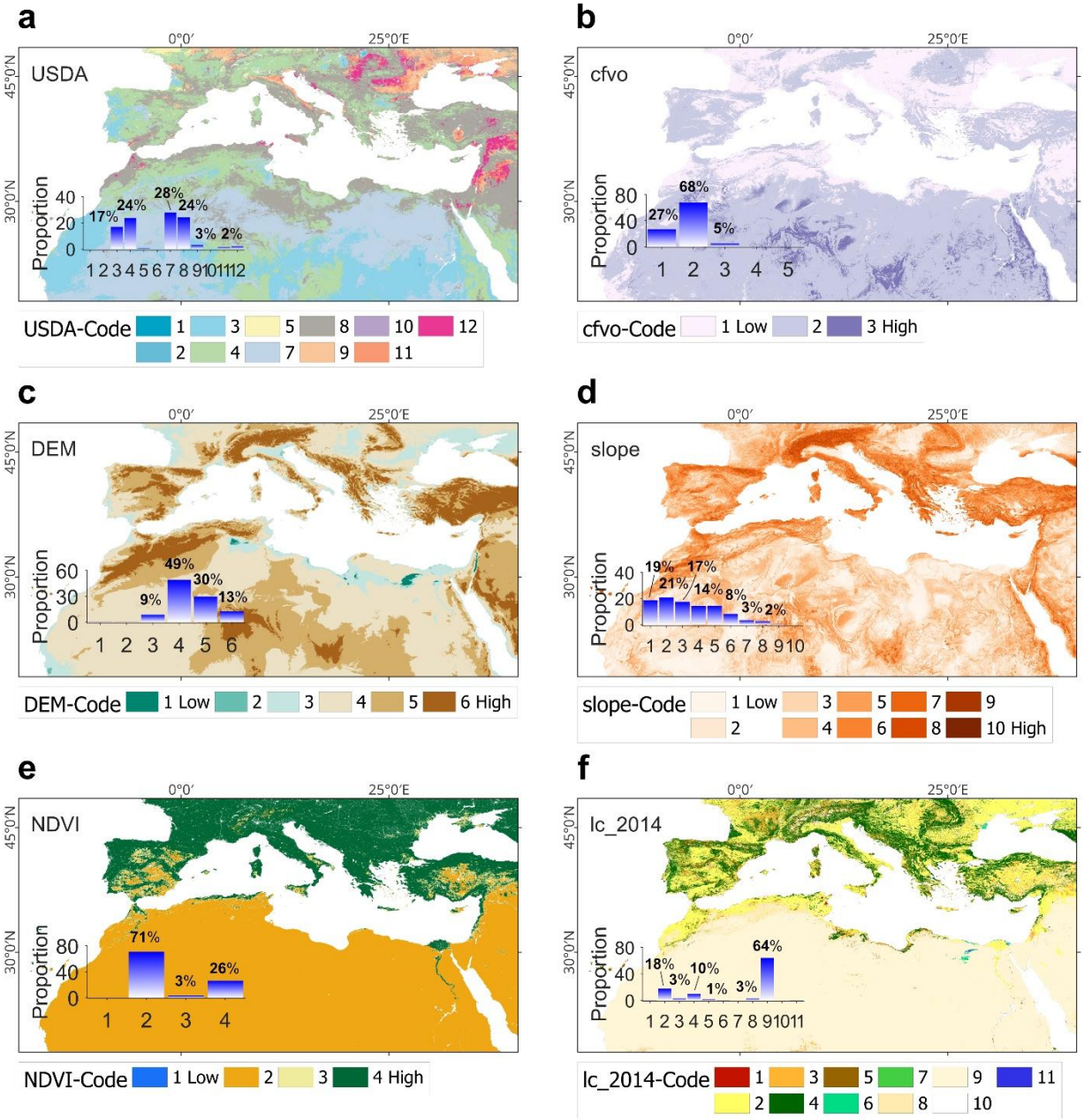
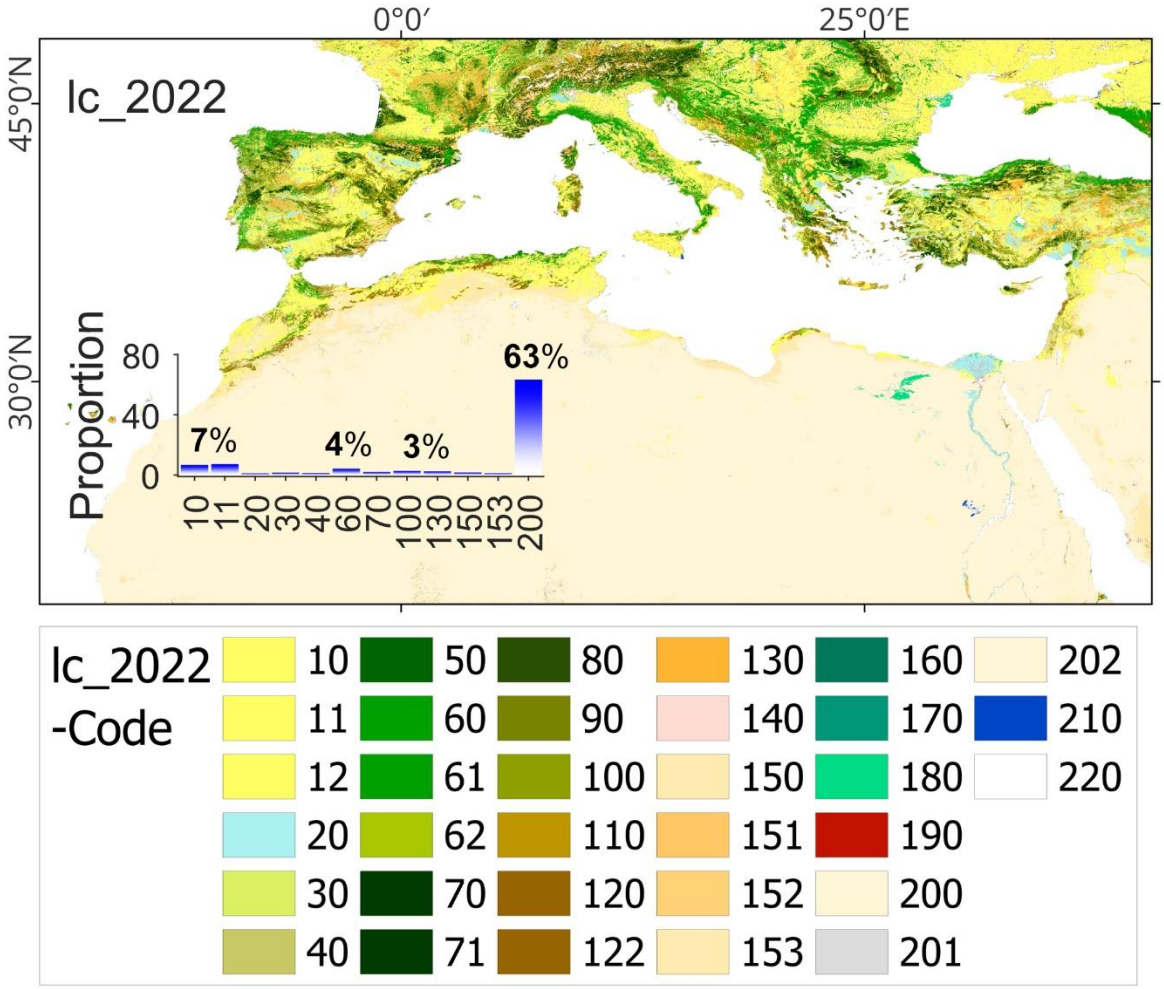


Fig. 2. Mediterranean-wide environmental zonation of abiotic environmental characteristics based on literature-informed classification. ***a****, soil texture (USDA; sand, silt, clay),* ***b****, coarse fragments content (cfvo),* ***c****, elevation (DEM),* ***d****, surface slope (slope),* ***e****, vegetation cover seasonality (NDVI),* ***f****, land cover (lc_2014). Classification code ranges are provided in Supplementary Table 3. Bar charts show the proportion of area within each class.*



Extended Data Fig. 2. Mediterranean-wide environmental zonation of land-cover classes. *Classification of land cover (lc_2022). Classification code ranges are provided in Supplementary Table 4. Bar charts show the proportion of area within each class.*

Current and future climatic constraints

Precipitation (pr) and reference/potential evapotranspiration (eto_hs) patterns for the 2000-2019 (**Fig. 3** and Supplementary Table 5, Supplementary Table 6), together with clustered projections for 2041–2060 under SSP2-4.5 and SSP5-8.5 (**Fig. 3** and Supplementary Table 7–Supplementary Table 8, Supplementary Table 9–Supplementary Table 10), reveal pronounced spatial gradients in climatic water availability across the Mediterranean basin. Precipitation and reference evapotranspiration maps capture basin-scale climate patterns (**Fig. 3**). The baseline period (2000–2019) exhibits a clear latitudinal gradient, with the highest rainfall occurring across the northern Mediterranean and major mountain systems, including northern Spain, the Pyrenees, Massif Central, Alps, northern Apennines, Dinaric Alps, and western Balkans. Precipitation progressively declines toward the southern and

eastern margins of the basin, particularly across the southern Iberian Peninsula, Sicily, the Maghreb interior plains, the Libyan Desert margin, the Sinai Peninsula, and the Levantine corridor. Evapotranspiration exhibits an inverse pattern, increasing toward the south and reaching its highest values across the Sahara, particularly in the Tanezrouft Basin, Libyan Desert, and Western Desert of Egypt. Under SSP2–4.5 and SSP5–8.5, projected precipitation declines and evapotranspiration increases are spatially coherent, leading to intensified water deficits, especially across semi-arid transition zones such as Andalusia, Murcia, the High Plateaus of Algeria, the Sahel Atlas margins, central Tunisia, the Thessaly Plain, the Anatolian Plateau, and the Syrian Steppe. SSP5–8.5 exhibits broader low-precipitation zones, indicating compounding hydrological stress rather than uniform drying (**Fig. 3**).

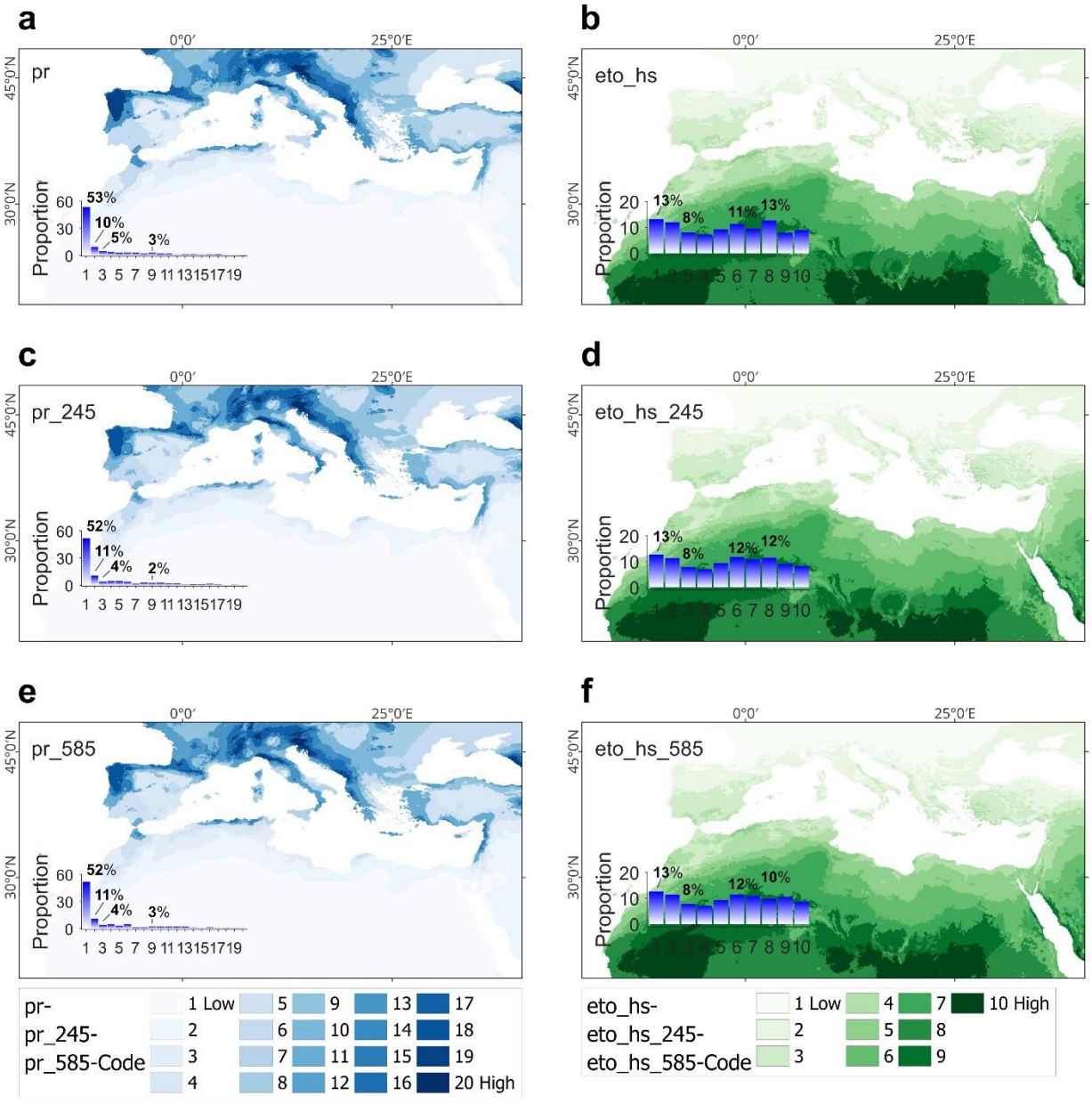


Fig. 3. Mediterranean-wide environmental zonation of abiotic environmental climatic parameters based on unsupervised clustering. a-b *Classification of climatic parameters for the recent past period (2000-2019):* ***a****, recent past precipitation (pr),* ***b****, recent past reference/potential evapotranspiration (eto_hs).* ***c-d*** *Classification of climatic parameters under the SSP2–4.5 climatic scenario for the period 2041–2060:* ***c****, future precipitation (pr_245),* ***d****, future reference/potential evapotranspiration (eto_hs_245).* ***e-f*** *Classification of climatic parameters under the SSP5–8.5 climatic scenario for the period 2041–2060:* ***e****, future precipitation (pr_585),* ***f****, future reference/potential evapotranspiration (eto_hs_585). Classification code ranges are provided in Supplementary Table 5 –Supplementary Table 10. Bar charts show the proportion of area within each class.*

Spatial distribution of marginal lands and opportunity spaces

We selected soil health indicators (Supplementary Table 11) and compiled reference values to rank Mediterranean soil health.

Constraints associated with soil acidity, alkalinity, and salinity were concentrated in specific Mediterranean hotspots (Fig. 4 and Supplementary Table 12). Low SOC was particularly concentrated in arid and semi-arid regions, including the Libyan Desert margin, Eastern Algeria High Plateaus, Sinai Peninsula, and Syrian steppe (Fig. 4 and Supplementary Table 13). High bulk-density constraints were concentrated in Central Tunisia, the Jordan Rift Valley, Bekaa Valley, Lebanon Mountains, the Syrian Steppe, and the Carpathian foothills (**Fig. 4** and Supplementary Table 13).

Low RCI and CEC values, indicative of reduced intrinsic soil productivity, and low AI values, associated with increasing aridity, were concentrated across Mediterranean climatic transition belts, including the Meseta Central, Andalusia, Murcia, central Tunisia, the High Plateaus of Algeria, Sahel Atlas margins, the Thessaly Plain, Central Anatolia, and the Syrian Steppe (**Fig. 4** and Supplementary Table 14). Comparable patterns were observed under both future climate scenarios (SSP2-4.5 and SSP5-8.5) (**Fig. 4**; Extended Data Fig. 4).

Coarse-fragment constraints were predominantly associated with mountainous regions, including the Atlas Mountains, Rif Mountains, Alps, Apennines, Pyrenees, and Taurus Mountains (**Fig. 4** and Supplementary Table 15).

Areas classified as unhealthy based on NDVI were concentrated in desert and dryland systems, including the Tanezrouft Basin, Western Desert of Egypt, Negev Desert, and Syrian Desert, reflecting sparse vegetation cover and low ecosystem productivity (**Fig. 4** and Supplementary Table 15). Topographic constraints were limited in areas below mean sea level, primarily represented by the

Dead Sea Depression, but were widespread in mountainous regions, including the Atlas Mountains, Alps, Apennines, Pyrenees, and Balkan Mountains, where medium-to-steep slopes predominated (**Fig. 4** and Supplementary Table 16). Land-cover types associated with poor soils, shrublands, sparse vegetation, and areas with flooded water, freshwater/saline/brackish water, or bare ground were classified as unhealthy (**Fig. 4** and Supplementary Table 17). These patterns are common in arid transition zones (e.g., Chott El Jerid basin, Maghreb Interior Plains, Syrian steppe) and are widespread along European coasts and inland areas, indicating low or patchy vegetation cover based on ESA CCI (2022). Unhealthy precipitation clusters were associated with semi-arid to arid conditions, characterized by mean annual precipitation below 500 mm or particularly low precipitation during the April–September period (**Fig. 4** and Supplementary Table 18).

These conditions are widespread across Mediterranean dryland belts, extending from the southern Iberian Peninsula to the Levantine interior through the Sahel Atlas margins, central Tunisia, the Cyrenaica Plateau, and the Sinai Peninsula. Additional hotspots occur across the Sahara, southern Italy, and the Vardar Basin. Similar classifications for SSP2-4.5 and SSP5-8.5 scenarios (2041–2060) are documented in Supplementary Table 19 and Supplementary Table 20, as well as **Fig. 4** and Extended Data Fig. 4.

The analysis of soil health percentages (**Fig. 4**) shows class distribution across parameters for marginal land identification. The harmonized datasets exhibit only negligible differences in spatial extent, resolution, and coverage, with a maximum discrepancy of approximately 1%. This result confirms that coverage harmonization has no meaningful impact on classification quality across the various scenarios examined.

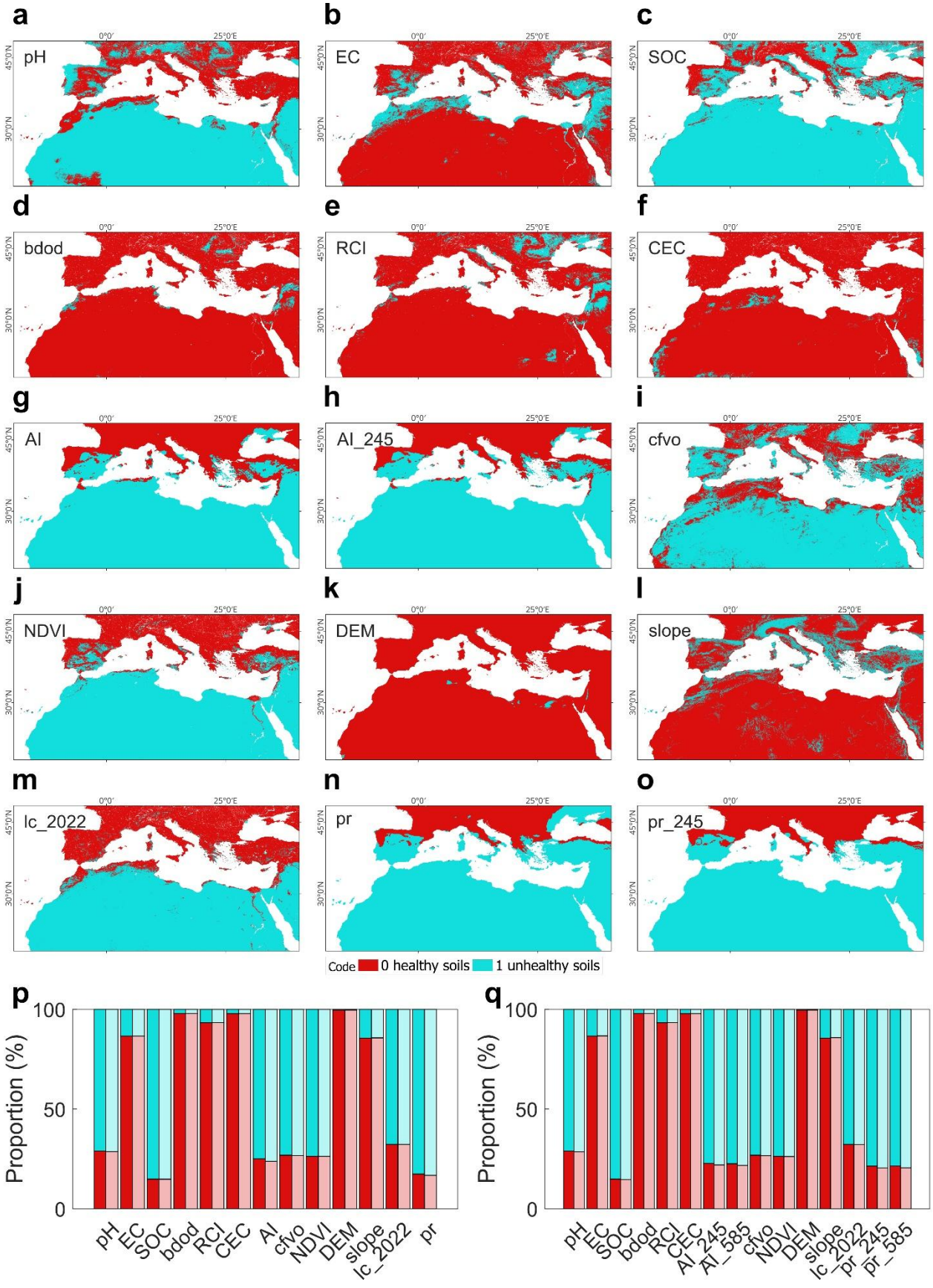
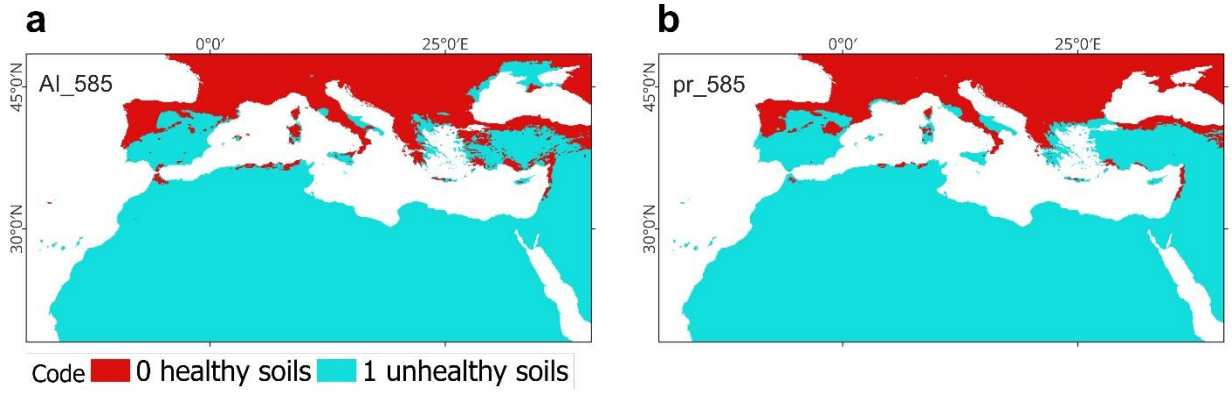


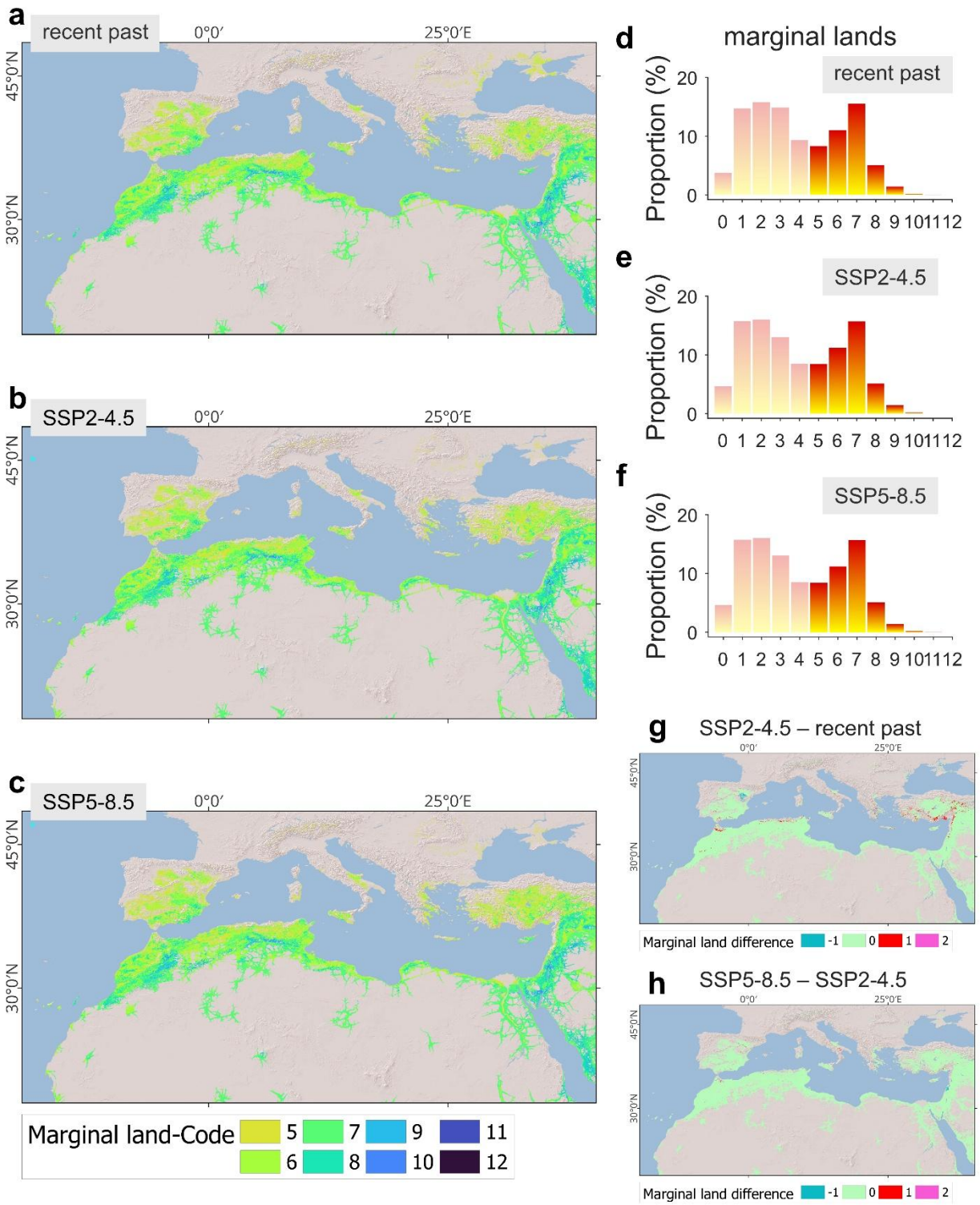
Fig. 4. Distribution of healthy and unhealthy soils. *Binary ranking of abiotic and climatic indicators:* ***a****, soil acidity (pH),* ***b****, soil salinity (EC),* ***c****, soil organic carbon (SOC),* ***d****, soil bulk density*

*(bdod); **e**, retention curve index (RCI), **f**, soil cation exchange capacity (CEC), **g**, recent past aridity index (AI; 2000–2019), **h**, future aridity index (AI_245; 2041–2060), **i**, coarse fragments content (cfvo), **j**, vegetation cover seasonality (NDVI), **k**, elevation (DEM), **l**, surface slope (slope), **m**, land cover (lc_2022), **n**, recent past precipitation (pr; 2000–2019), **o**, future precipitation (pr_245; 2041–2060). Rank "0" (red color) denotes healthy soil, and rank "1" (blue color) denotes unhealthy soil, representing limitations for conventional agriculture and potential target environments for NUS. Classification code ranges are provided in Supplementary Table 12–Supplementary Table 20. The bar charts show the proportions of 1-Code and 0-Code across the harmonized datasets in terms of spatial extent and resolution (full color) and coverage (shaded color) for the recent past (**p**) and future scenarios (**q**).*



***Extended Data Fig. 4. Distribution of healthy and unhealthy soils.** Binary ranking of abiotic and climatic indicators: **a**, future aridity index (AI_585; 2041–2060), **b**, future precipitation (pr_585; 2041–2060). Rank "0" (red color) denotes healthy soil, and rank "1" (blue color) denotes unhealthy soil, representing limitations for conventional agriculture and potential target environments for NUS. Classification code ranges are provided in Supplementary Table 14 and Supplementary Table 20.*

Marginal land classes were derived by aggregating soil-health rankings into a cumulative score from 0 (healthy across all parameters) to the maximum number of parameters classified as unhealthy, thereby identifying areas with increasing abiotic constraints and higher marginality. Areas with limited accessibility (travel time > 3 h) were then masked out following [12]. Marginal-land maps were produced for the baseline period 2000–2019 and for future projections under SSP2-4.5 and SSP5-8.5 (2041–2060) (**Fig. 5** and Supplementary Fig. 2).



295

296 ***Fig. 5. Marginal lands under recent past and future scenarios.*** *Classification of marginal lands*
297 *above the critical threshold of five "unhealthy" parameters mapped within areas reachable from an*
298 *urban center within a 3-hour travel-time cutoff for* ***a****, recent past (2000–2019),* ***b****, SSP2–4.5 (2041–*
299 *2060),* ***c****, SSP5–8.5 (2041–2060). Values represent the cumulative number of "unhealthy"*
300 *parameters. Bar charts show the proportion of area within each marginality class for* ***d****, recent past*
301 *(2000–2019),* ***e****, SSP2–4.5 (2041–2060),* ***f****, SSP5–8.5 (2041–2060); full color indicates classes above*

the critical threshold, thus considered as marginal, and color shading indicates classes below the critical threshold not considered as marginal. ***g-h****, display the difference in the marginality classification of marginal lands above the critical threshold between* ***g****, future scenario SSP2–4.5 (2041–2060), and recent past (2000–2019),* ***h****, future scenario SSP5-8.5 and SSP2–4.5 (2041–2060). The positive values indicate an increase in the number of marginality classes. Basemaps in* ***a, b, c, g, h*** *are from ESRI.*

The baseline marginal map (2000–2019) with a critical threshold of 5 aggregated unhealthy parameters for marginal lands (Supplementary Note S 2), reveals that more than 40% of the areas within a 3-hour travel-time from the nearest urban center are marginal lands, corresponding to almost 1.83 million km² at a medium latitude (2.58 million km² not marginal) (**Fig. 5**). High cumulative-stress zones are concentrated along the southern Mediterranean margins, particularly in the southern Iberian Peninsula, Sicily, Crete, Cyprus, and the Cyrenaica coast. Additional hotspots are found in semi-arid and arid regions, including the High Plateaus of Algeria, central Tunisia, the Anatolian Plateau, and the Syrian Steppe, as well as in coastal areas affected by salinity, notably the Nile Delta, Gulf of Gabès, and Chott el Jerid basin. These marginal lands form a continuous belt of high marginality, driven by a combination of limiting factors, including aridity, salinity, SOC, land cover, NDVI, slope, and coarse fragments.

Marginal land maps for 2050 under SSP-2.45 and SSP-5.85 closely resemble recent-past scenarios, showing persistent marginalization patterns (**Fig. 5** and Supplementary Fig. 2). Marginalized areas show little improvement due to fixed abiotic constraints (DEM, slope, pH, soil bulk density) and gradual climate change. Climate marginality zones expand slowly, with high-constraint areas remaining largely unchanged between 2000–2019 and 2050.

Regionally, marginal-land trends vary under future climate scenarios. Under SSP2–4.5, marginal land expands in the Sahel Atlas margins, Thessaly Plain, and southern Anatolia, primarily in response to increasing climatic constraints (**Fig. 5**), while localized reductions occur in parts of the eastern Iberian Peninsula. Under SSP5–8.5, marginal land expands further, particularly in southern Italy, with additional hotspots emerging in Iberia and the Thessaly Plain. The overall expansion of marginal land is approximately 16 thousand km² under SSP2–4.5 and 22 thousand km² under SSP5–8.5 (**Fig. 5**), suggesting that future changes are likely to be concentrated in environmentally sensitive transition zones rather than uniformly distributed across the Mediterranean basin.

Discussion

This study presents a Mediterranean-wide geospatial framework designed to support the assessment of agroecological opportunity spaces for NUS. By converting heterogeneous open datasets into a consistent, decision-oriented environmental baseline, the framework enables standardized comparisons across countries and biophysical contexts, facilitating the transition from site-specific applications toward broader transferability, replication, and coordinated upscaling. Beyond its technical contribution, this framework provides information that may support the assessment of resilience-oriented land-use strategies aligned with climate adaptation and land degradation neutrality objectives.

Variable selection was informed by leading agendas on soil health, water security, land degradation neutrality, and sustainable food systems, translating shared priorities into spatially explicit indicators of soil functioning, water availability, and land constraints. A key contribution of the framework is the identification of abiotic soil and climatic stress gradients across countries, which may inform the transferability of diversification strategies for species adapted to salinity, aridity, and nutrient-poor substrates. This transferability is reinforced by the use of globally consistent and reproducible datasets, which are intended to minimize the risk that observed patterns reflect differences in national data availability rather than underlying environmental conditions.

The observed patterns of soil acidity, alkalinity, bulk density, and organic carbon are consistent with major Mediterranean pedogenic gradients shaped by parent material, climate, and land-use pressures. In several dryland regions, the co-occurrence of soil compaction and low organic carbon suggests compounded constraints that may further limit soil functioning and agricultural productivity. The concentration of coarse-fragment-rich soils in mountainous environments highlights areas where shallow soil depth and terrain constraints may limit conventional agricultural practices, while potentially favoring stress-adapted perennial species. The coexistence of high SOC and strong topographic constraints in mountainous regions further illustrates that favorable soil properties alone may be insufficient to overcome other environmental limitations. The spatial distribution of CEC suggests that nutrient-retention limitations may reinforce climatic and soil constraints in several Mediterranean drylands, particularly where low exchange capacity co-occurs with aridity and reduced organic carbon levels. Conversely, relatively high CEC values observed in some hyper-arid regions do not necessarily indicate favorable soil fertility, as severe water limitation and low organic matter inputs may constrain the functional expression of this potential. The occurrence of very high RCI values in hyper-arid regions highlights the importance of interpreting individual indicators within their broader environmental context. Although these areas exhibit favorable texture-related physical

properties, severe climatic water limitations may override this potential, limiting the agronomic expression of otherwise suitable soil conditions. This finding reinforces the need to evaluate soil and climatic indicators jointly when identifying agroecological opportunity spaces.

Importantly, the spatial patterns identified here reveal a mismatch between current land use and environments potentially suitable for stress-adapted species, suggesting that areas considered marginal for conventional agriculture may represent agroecological opportunity spaces for diversification. The mapped land marginality should therefore be interpreted as a basin-scale abiotic screening tool that may help identify environmental opportunity spaces for further species-specific evaluation, rather than as a direct predictor of crop performance or agronomic suitability.

A key conceptual aspect of this work is to reframe marginal lands not as residual or degraded areas but as agroecological opportunity spaces where stress-adapted NUS may support diversification under environmental constraints that limit conventional agriculture.

The persistence of sparse vegetation and shrubland communities across several marginality hotspots indicates that, despite abiotic constraints, these environments can still support biological productivity. This observation supports exploring stress-adapted diversification strategies, such as the introduction of NUS, in these areas.

Notably, the results indicate modest but consistent increases in aridity across transitional semi-arid belts (e.g., Andalusia, central Tunisia, the High Plateaus of Algeria, the Thessaly Plain, and Central Anatolia). Although projected shifts in class proportions remain limited, even small changes in water balance may have disproportionate effects in these environmentally sensitive regions. As precipitation and evapotranspiration jointly regulate soil-moisture availability, declining rainfall and increasing atmospheric water demand may intensify soil desiccation and further constrain agricultural productivity in already vulnerable semi-arid environments [13,14]. The concentration of future marginality increases within semi-arid transition zones may support the exploration of stress-adapted diversification strategies, including NUS, as part of broader climate-adaptation pathways.

The concentration of salinity-related constraints in coastal plains, inland depressions, and arid Mediterranean regions highlights environments where salt accumulation may further limit conventional agricultural productivity and where salt-tolerant NUS may warrant further evaluation as diversification options [15–17].

The deployment of NUS in marginal lands is not without trade-offs. Although these species may enhance resilience and diversify production systems, their expansion could interact with water use, ecosystem services, and land-management priorities in complex ways. For example, increased

biomass production in water-limited environments may alter fragile ecological equilibria, while halophyte cultivation in saline or coastal systems could compete with conservation objectives [15,16]. These considerations highlight the need to complement abiotic opportunity mapping with ecological, socioeconomic, and governance assessments.

The identified opportunity spaces, which largely overlap with Mediterranean transition zones, are already exposed to water scarcity, soil degradation, and increasing climate risks. Prioritizing these areas for NUS-based diversification may support the exploration of strategies relevant to climate adaptation, land degradation neutrality, and food-system resilience. By identifying environmental analogues across national boundaries, the framework may inform the assessment of diversification strategies across the Mediterranean region.

Several limitations should be acknowledged. The framework focuses on abiotic and climatic conditions and does not account for species-specific requirements, infrastructure, market access, biotic pressures, or broader socioeconomic factors that influence NUS adoption. Climate projections are based on multi-model averages and therefore do not explicitly represent inter-model uncertainty. In addition, the threshold of five unhealthy parameters should be regarded as an operational screening criterion rather than a universal definition of land marginality. The binary classification of soil health and additive aggregation of indicators simplifies complex ecological gradients and may not fully capture interactions among soil, climate, and vegetation processes. Finally, while the basin-scale resolution is appropriate for regional assessments, it may overlook fine-scale heterogeneity relevant to local decision-making. Future work should integrate uncertainty analyses, field validation, socioeconomic information, and species-specific assessments to improve prioritization and local applicability.

The proposed framework provides a reproducible and transparent basis for identifying climate-resilient diversification opportunity spaces across Mediterranean agrifood systems. Rather than delineating fixed suitability zones, the approach identifies environmental opportunity spaces where stress-adapted species can be considered under increasing climatic constraints. Coupling basin-scale environmental screening with field validation, socioeconomic information, and species-specific assessments will be essential to translate these opportunities into actionable pathways for resilient agrifood transitions across the Mediterranean.

Methods

Geospatial database and environmental variables

Public geospatial databases covering key abiotic factors relevant to agricultural production were systematically explored and evaluated across the Mediterranean Basin (Supplementary Table 21). The methodological workflow used for Mediterranean-wide marginal-land mapping is summarized in Supplementary Fig. 3. The workflow integrates geospatial datasets, derived indicators, classification procedures, and marginality assessment to characterize environmental constraints and identify agroecological opportunity spaces that may warrant further evaluation for diversification strategies involving stress-adapted NUS.

Variable selection was informed by internationally recognized frameworks related to soil health, water security, land degradation neutrality, climate adaptation, and sustainable food systems. Priority was given to indicators with demonstrated ecological relevance, Mediterranean-wide coverage, reproducibility, and long-term availability. The selected variables encompass soil chemical properties (pH, EC, SOC, and CEC), soil physical properties (bdod, RCI, texture fractions, and coarse fragments) topography (DEM and slope), vegetation cover seasonality (NDVI), land cover, and climatic indicators, including precipitation, reference evapotranspiration (ET_o), and the Aridity Index (AI) (Supplementary Table 22). Candidate datasets were evaluated based on parameter availability, spatial coverage, spatial resolution, usability, and publication year to prioritize products that combine basin-wide consistency, methodological transparency, and reproducibility. This approach minimizes the risk that observed patterns reflect differences in data availability or processing workflows rather than underlying environmental gradients.

The final database included ISRIC products for soil properties, WorldClim v2.1 [18] for climate variables, FAO and ESA Climate Change Initiative products for land cover, TanDEM-X for topographic information, and the USGS EarthExplorer archive for NDVI. Soil parameters were extracted for the 0–5 cm, 5–15 cm, and 15–30 cm layers, consistent with the typically shallow rooting depth of many NUS considered for Mediterranean diversification strategies.

Climate variables were analyzed for the recent past (2000–2019) using CRU-TS 4.09 [19] downscaled with WorldClim 2.1 and for future conditions (2041–2060) using ensemble CMIP6 projections from thirteen global climate models (ACCESS-CM2, BCC-CSM2-MR, CMCC-ESM2, EC-Earth3-Veg, FIO-ESM-2-0, GISS-E2-1-G, HadGEM3-GC31-LL, INM-CM5-0, IPSL-CM6A-LR, MIROC6, MPI-ESM1-2-HR, MRI-ESM2-0, and UKESM1-0-LL) under SSP2–4.5 and SSP5–8.5 scenarios.

Particular emphasis was placed on precipitation and reference evapotranspiration, which together represent the primary climatic controls on soil moisture dynamics and agricultural water availability.

Several derived indicators were subsequently computed from the assembled soil, topographic, and climatic datasets to better represent processes controlling soil functioning and environmental stress, including water retention, carbon stabilization, nutrient retention, erosion susceptibility, and climatic water limitation. These indicators are described in the following section.

Derived indicators of soil functioning and climatic stress

Several indicators were derived from the assembled soil, topographic, and climatic datasets to better represent processes controlling soil functioning and environmental stress. These indicators complement the primary variables by quantifying key mechanisms related to soil physical quality, carbon stabilization, water retention, erosion susceptibility, nutrient retention, and climatic water limitation.

Depth-weighted average of soil parameters (0–30 cm)

To represent near-surface conditions relevant to plant establishment and early growth, each soil variable was aggregated over the 0–30 cm profile using a thickness-weighted mean of the 0–5 cm, 5–15 cm, and 15–30 cm layers. This approach provides a single representative topsoil value while minimizing biases associated with unequal depth intervals.

Slope

Slope was derived from the TanDEM-X digital terrain model using a local plane-fitting approach within a moving window. The resulting layer captures terrain inclination and localized steep gradients relevant to runoff generation, erosion processes, and land-use constraints.

Retention Curve Index (RCI)

The Retention Curve Index (RCI) is a texture-based indicator of intrinsic soil physical quality that reflects soil productivity and workability under idealized conditions, independent of limitations imposed by water availability, nutrient supply, climate, pests, or diseases [20]. The index builds upon Dexter's S-index, defined as the slope at the inflection point of the soil water retention curve and widely used as an indicator of soil physical quality for root growth and tillage operations [21–23].

Following [21–23], RCI was calculated using the relationship between clay content and Dexter's S-index established for the twelve USDA/FAO texture classes [24]. The resulting function identifies an optimal clay content of approximately 20%, corresponding to the maximum physical soil quality. RCI values

were subsequently rescaled between 0 and 1, where values approaching 1 indicate optimal texture-related physical conditions and values approaching 0 indicate increasingly suboptimal conditions

$$RCI = 1 - \{abs(S_i - S_{opt})/(S_{max} - S_{opt})\} \quad (1)$$

where $S_i = f(Clay\%) = 0.0713 * (Clay\%)^{-0.238}$, S_{opt}= 0.035 and S_{max}= 0.1233

considering that the S value of 0.035 is the optimum value (value 1 in the RCI function), while 0 corresponds to the S value with the maximum distance from Sopt (i.e., Smax).

Mineral-associated organic carbon (MAOC)

To contextualize the status of soil organic carbon, we estimated mineral-associated organic carbon (MAOC), also referred to as soil organic carbon saturation (SOCS). MAOC represents the capacity of soils to stabilize organic carbon through associations with the fine mineral fraction (silt + clay) and provides a texture-dependent benchmark that is largely independent of climate and land use.

As an indicator of the potential for additional stable carbon storage, MAOC/SOCS provides a texture-based benchmark that is largely independent of climate and land use. The concept was originally introduced by [25] and has since been widely applied thereafter [26–28]. In this study, MAOC (Supplementary Fig. 4) was estimated using the linear model proposed by [27]:

$$MAOC\left(\frac{g}{kg}\right) = 0.78 * (Silt\% + Clay\%) \quad (2)$$

where silt and clay represent the percentage contents of the respective particle-size fractions.

Reference evapotranspiration (ET_o)

ET_o was estimated using the temperature-based Hargreaves–Samani formulation [29,30], adopting the globally corrected version proposed by [31]. This correction incorporates spatially explicit calibration factors derived from global datasets and benchmarked against the revised FAO-56 short-crop approach.

Daily ET_o values were converted to monthly values using the exact number of days per month. Additional filters were applied under frost conditions to improve global robustness. Extraterrestrial radiation and associated astronomical parameters were calculated following [32].

The adjusted equation is:

$$ET_o = c_{hs2} \cdot (T_{mean} + 17.8) \cdot \frac{R_a}{\lambda} \cdot (TD)^{0.5} \quad (3)$$

where $ET_o$is reference evapotranspiration (mm d^{-1}); $R_a$is extraterrestrial radiation (MJ m^{-2} d^{-1}); $\lambda$is latent heat of vaporization (2.45 MJ kg^{-1}; $1/\lambda = 0.408$) [33]; $T_{mean}$is mean daily air temperature

(°C); TD is the daily temperature range ($T_{max} - T_{min}$); and c_{hs2} is a location-specific correction factor from the global dataset of [31] for the short reference crop. Daily ET_o values were converted to monthly values by multiplying each by the exact number of days in the month. Two filters were applied to ensure global robustness under frost conditions: (i) when $T_{mean} < -17.8$°C, (T_{mean}+17.8) was set to zero [34]; and (ii) ET_o was set to zero when $T_{max} \leq 0$°C, reflecting extreme frost conditions. The extraterrestrial radiation was calculated by the following formulas [32]:

$$R_a = \frac{24}{\pi} G_{sc} d_r [(\omega_s) \cdot sin\,\varphi \cdot sin\,\delta \cdot + cos\,\varphi \cdot cos\,\delta \cdot (\omega_s)] \quad (4)$$

where R_a is extraterrestrial radiation (MJ m^{-2} d^{-1}); G_{sc} is the solar constant (4.92 MJ m^{-2} h^{-1}); d_r is the inverse relative Earth–Sun distance factor (–); ω_s is the sunset hour angle (rad); φ is latitude (rad); and δ is solar declination (rad). Latitude is positive in the Northern Hemisphere and negative in the Southern Hemisphere. Conversion from decimal degrees to radians follows:

$$Radians = \frac{\pi}{180} \times decimal\ degrees \quad (5)$$

The remaining parameters of the extraterrestrial radiation are provided by the following formulas:

$$\delta = 0.409\ sin\left(\frac{2\pi}{365} J - 1.39\right) \quad (6)$$

dr = 1 + 0.033cos(2πJ/365)

ωs = arccos[-tan(φ)×tan(δ)]

J is the day number in the year, ranging from 1 (1 January) to 365 or 366 (31 December). For monthly periods, J can be calculated.

$$J = Int(30.4M - 15) \quad (7)$$

where M is the month number (1-12).

Aridity Index (AI)

Climatic water limitation was quantified using the United Nations Environment Programme (UNEP) Aridity Index (AI), defined as the ratio between annual *Py* to annual potential/reference evapotranspiration *ETo*y [35,36]. This index is widely used to characterize climatic aridity and distinguish among humid, dry sub-humid, semi-arid, arid, and hyper-arid environments:

$$AI_{UNEP} = \frac{P_y}{ET_{oy}} \quad (8)$$

Following the calculation of derived indicators, all datasets were harmonized in spatial extent, coordinate reference system, and resolution to support Mediterranean-wide analyses. The final study

domain extended from −19.5°E, 48.5°N to 40.5°E, 18°N in EPSG:4326 (WGS84). Whenever possible, datasets were retained at their native spatial resolution to preserve thematic integrity and avoid artificial increases in spatial precision. Resolution harmonization was applied only when generating aggregated marginality outputs.

For soil variables, a resolution of 30 arc-seconds was adopted, whereas climate variables retained their native 5 arc-minute resolution. Previously classified products, including salinity and land-cover datasets, were maintained at their original resolutions because interpolating categorical information can introduce substantial inaccuracies. Vegetation and land-cover layers were additionally masked using the common spatial extent of the soil databases to ensure spatial consistency across all analyses.

Classification and environmental zonation

Environmental variables (Supplementary Table 23) were classified using literature-based thresholds, established soil-quality criteria, percentile distributions, or equal/geometric interval approaches, depending on the indicator. This strategy enabled the comparison of variables expressed in different units and scales while preserving their ecological interpretation. Season-independent variables, including soil and topographic properties, were classified according to published thresholds or statistical distributions, whereas season-dependent climatic variables were grouped using cluster-based approaches. The resulting classifications provided a standardized basis for identifying environmental gradients and spatial patterns of abiotic constraints across the Mediterranean Basin.

Soil acidity and salinity

Soil acidity (pH) and salinity (EC) were classified using published thresholds [37–39] describing plant responses to soil chemical conditions. Classification results and their spatial distributions are reported in **Fig. 1** and Supplementary Table 1. For the marginal-land assessment, very strongly to moderately acidic soils (pH < 5.3), alkaline soils (pH > 7.8), and soils exhibiting slight to extreme salinity (EC > 2 dS m^{-1}) were classified as unhealthy according to the adopted binary ranking scheme (**Fig. 4,** Supplementary Table 12).

Soil organic carbon

Soil organic carbon (SOC) was classified using a mineral-associated organic carbon (MAOC) framework. Because MAOC depends primarily on soil texture, it provides a consistent benchmark for evaluating SOC status across contrasting climatic and land-use conditions. Classification results are summarized in **Fig. 1** and Supplementary Table 1. For marginal-land identification, soils

containing less than 50% of their estimated MAOC capacity (SOC < 0.5 MAOC) were classified as unhealthy (**Fig. 4,** Supplementary Table 13).

Soil bulk density

Bulk density (bdod) was classified according to texture-specific thresholds proposed by the Soil Survey Staff [40] for the twelve USDA/FAO texture classes [24] (Supplementary Table 24). This approach accounts for the fact that acceptable bulk-density values vary substantially among soil textures. This method defines three bulk-density thresholds: bdod < R1 (ideal), bdod = R2 (potential limitations), and bdod > R3 (restricted plant/root growth). Classification results are summarized in **Fig. 1** and Supplementary Table 1. For marginal-land identification, soils exceeding the R2 threshold were classified as unhealthy because they may experience increasing physical limitations to root development and soil functioning (**Fig. 4,** Supplementary Table 13).

Retention Curve Index and Cation Exchange Capacity

Retention Curve Index (RCI) and cation exchange capacity (CEC) were used as indicators of intrinsic soil productivity, representing the texture-related physical–hydraulic and chemical capacity of soils to support plant growth. RCI was classified using the 90th, 75th, 50th, and 25th percentiles of its distribution, whereas CEC was classified according to thresholds proposed by [41]. Classification results are summarized in **Fig. 1** and Supplementary Table 2. For marginal-land identification, areas with RCI < 0.945 and CEC < 12 cmol(+) kg^{-1} were classified as unhealthy according to the adopted binary ranking scheme (**Fig. 4,** Supplementary Table 14).

Aridity Index

The UNEP Aridity Index (AI) was used as an indicator of climatic productivity potential and water limitation. AI classes were defined using internationally recognized UNEP thresholds [35], with minor adjustments to the upper- and lower-class limits to better represent Mediterranean climatic gradients productivity [36,42,43]. Classification results are summarized in **Fig. 1** and Supplementary Table 2. Areas with AI < 0.50 were classified as unhealthy for conventional agricultural production (**Fig. 4,** Supplementary Table 14).

Soil texture and coarse fragments

Soil texture is defined by the mass fraction of sand, silt, and clay in the fine-earth fraction (< 2 mm) [44]. In the USDA system, particle-size limits are: sand (2.0–0.05 mm), silt (0.05–0.002 mm), and clay (< 0.002 mm); a combination of these fractions defines 12 texture classes [38]. The resulting texture classification is summarized in Supplementary Table 3 and mapped in **Fig. 2**. Coarse fragment content (cfvo) (> 2 mm) was classified by abundance (%) following [44] and [38]. Classification thresholds

and corresponding maps are reported in **Fig. 2** and Supplementary Table 3. For marginal-land identification, areas with more than 15% coarse fragments were classified as unhealthy because high coarse-fragment abundance may reduce effective rooting volume and decrease soil water- and nutrient-storage capacity (**Fig. 4,** Supplementary Table 15).

Topography

Topography elevation (dem) was classified following [45,46], whereas surface slope (slope) derived from the TanDEM-X DEM was classified using [37] thresholds. Classification results are summarized in **Fig. 2** and Supplementary Table 3. For marginal-land identification, areas below mean sea level and those with slopes exceeding 5% were classified as unhealthy due to potential constraints related to drainage conditions, erosion risk, and mechanized agricultural operations (**Fig. 4,** Supplementary Table 16).

Vegetation cover seasonality

Vegetation cover seasonality (NDVI), computed from red (RED) and near-infrared (NIR) reflectance was derived for the 2023–2024 period using monthly observations acquired between days 11 and 20 of each month to reduce single-date anomalies and ensure temporal consistency. Alternative metrics were evaluated, including annual maximum NDVI, annual mean NDVI, and summer (June-August) mean NDVI. The summer-average NDVI was retained because it provides a conservative representation of vegetation productivity under predominantly non-irrigated conditions and is generally less affected by cloud contamination. Areas with NDVI values below 0.3 were classified as primary-priority degraded environments, whereas areas with NDVI values below 0.4 were classified as secondary-priority environments. Classification results are summarized in **Fig. 2** and Supplementary Table 3. Low NDVI (i.e., NDVI < 0.3 as primary priority and NDVI < 0.4 as a lower priority) indicates sparse vegetation cover and reduced inputs that sustain soil biodiversity and organic matter, and was therefore ranked as unhealthy (**Fig. 4,** Supplementary Table 16).

Land cover

The land cover datasets for 2014 (lc_2014) and 2022 (lc_2022) capture land cover dynamics at different spatial resolutions and scales. For Mediterranean-wide assessments, the FAO dominant land cover dataset (30 arc-seconds), comprising 11 classes (lc_2014), was employed. For finer-scale, site-specific analyses (e.g., at national and local levels), including marginal land identification, the more recent ESA CCI land cover product (2022) with a spatial resolution of 300 m was used and reclassified into 33 classes (lc_2022). Classification results are reported in **Fig. 2**, Supplementary Table 3, and Extended Data Fig. 2, Supplementary Table 4. Land-cover types associated with poor

soils, shrublands, sparse vegetation, and areas with flooded water, freshwater/saline/brackish water, or bare ground were classified as unhealthy (**Fig. 4,** Supplementary Table 17).

Climatic zonation and K-means clustering

To characterize Mediterranean-scale climatic zonation, we applied K-means clustering (e.g., [47]) to the 12 mean monthly fields of recent-past precipitation and evapotranspiration (2000–2019) and to CMIP6 projections for SSP2-4.5 and SSP5-8.5 up to 2050 (2041–2060). Clustering was implemented using the SAGA-GIS K-Means Clustering for Grids tool within QGIS 3.34.12, adopting the Hill-Climbing approach [48]. We explored increasing the number of clusters until results stabilized, selecting 20 for precipitation and 10 for evapotranspiration. The procedure iteratively assigns grid cells to the nearest centroid and updates centroids until convergence [47,49]. Results for the recent past are summarized in Supplementary Table 5, Supplementary Table 6, and mapped in **Fig. 3**; projected clusters for SSP2-4.5 and SSP5-8.5 (2041–2060) are reported in Supplementary Table 7–Supplementary Table 8, Supplementary Table 9–Supplementary Table 10, and mapped in **Fig. 3**. Precipitation clusters were classified as unhealthy if their mean annual precipitation was less than 500 mm, or if April to September cumulative precipitation fell below those of the clusters below 500 mm per year threshold indicating semi-arid to arid water limitations (**Fig. 4,** Supplementary Table 18). Similar classifications for SSP2-4.5 and SSP5-8.5 scenarios (2041–2060) are documented in Supplementary Table 19 and Supplementary Table 20, as well as **Fig. 4** and Extended Data Fig. 4.

Marginal-land identification framework

Selection of soil health indicators

Marginal-land identification was based on a subset of abiotic and climatic indicators selected (Supplementary Table 22) to represent complementary dimensions of soil functioning, environmental stress, and agricultural constraints. To avoid redundancy among variables describing similar processes, indicators providing overlapping information were excluded from the final assessment. Consequently, mineral-associated organic carbon (MAOC), individual texture fractions (sand, silt, and clay), recent-past reference evapotranspiration (ET_o), and air-temperature variables (mean, minimum, and maximum temperature) were not included in the final marginality framework because their effects were already represented through derived or integrative indicators.

The final set of indicators (Supplementary Table 11) included soil pH, salinity (EC), soil organic carbon (SOC), bulk density (bdod), retention curve index (RCI), cation exchange capacity (CEC), coarse-fragment content (cfvo), elevation, slope, vegetation cover seasonality (NDVI), land cover, precipitation, and the UNEP Aridity Index (AI). Together, these variables capture major constraints

related to soil chemical and physical quality, climatic water availability, vegetation performance, and land-use suitability.

Ranking and harmonization approach

A binary ranking scheme was adopted to classify each indicator as healthy (0) or unhealthy (1) for conventional agricultural production. Thresholds were derived from published literature, established soil-quality criteria, statistical distributions, or climatic classifications, depending on the variable considered. The use of a binary framework enabled the integration of heterogeneous indicators into a common assessment structure while maintaining transparency and reproducibility.

Importantly, the terms "healthy" and "unhealthy" refer exclusively to suitability for conventional, input-intensive agricultural systems. Conditions classified as unhealthy indicate abiotic constraints that may reduce the performance of conventional crops. However, these same environments may represent priority areas for stress-adapted NUS and other climate-resilient diversification strategies. Consequently, the framework should be interpreted as an environmental screening approach rather than as a direct measure of crop suitability or productivity.

To represent soil conditions relevant to plant establishment, all soil variables were expressed as depth-weighted averages for the 0–30 cm profile. Individual binary rankings were subsequently aggregated to produce a cumulative constraint index, with each value representing the number of unhealthy conditions occurring at a given location.

To combine datasets originally available at different spatial resolutions, spatial harmonization procedures were applied only during the aggregation stage. Soil salinity was harmonized by using the maximum value within each aggregation unit to represent the most limiting condition, land-cover classes were aggregated using the modal value to preserve the dominant land-cover type, and climatic clusters were resampled using a nearest-neighbor approach. Coverage harmonization was subsequently applied to ensure spatial consistency across all layers included in the assessment.

Given the absence of a universally accepted weighting framework for Mediterranean-scale land marginality assessments, all indicators were assigned equal weight during the aggregation procedure. This parsimonious approach prioritizes transparency, reproducibility, and cross-country comparability while avoiding subjective assumptions regarding the relative importance of individual constraints.

Socio-economic parameters and critical thresholds

Socio-economic considerations were incorporated to identify areas where diversification strategies involving NUS may be realistically implemented (**Fig. 5**). Following previous studies, accessibility

was evaluated using travel-time proximity to urban centers [12]. Areas located within a three-hour travel time were considered potentially accessible for production, processing, and market integration activities.

The cumulative constraint index was then used to identify marginal lands. A threshold of five unhealthy indicators was adopted to define marginal conditions, thereby excluding locations characterized by only isolated or localized constraints. This threshold should be regarded as an operational screening criterion rather than a universal definition of land marginality.

The resulting framework identifies environments where multiple abiotic limitations co-occur and where conventional agricultural systems may face increasing constraints. Rather than delineating fixed suitability zones, the framework highlights agroecological opportunity spaces that may warrant further species-specific evaluation for climate-resilient diversification strategies involving stress-adapted NUS.

Data availability

The data used for this study are publicly available. Abiotic soil data (pH, SOC, bdod, CEC, clay, silt, sand, cfvo, EC) can be downloaded from the ISRIC-World Soil Information website (https://www.isric.org, https://data.isric.org/, https://files.isric.org/soilgrids/latest/data_aggregated/1000m). Vegetation cover seasonality (NDVI from eVIIRS 10-Day can be found on the USGS Earth Explorer (https://earthexplorer.usgs.gov), while DEM were obtained from Eurostat, the official website of the European Union. The product's original source is the TanDEM-X mission and has been produced by DLR e.V. (Distribution Airbus Defence and Space GmbH) (https://ec.europa.eu/eurostat/web/gisco/geodata/digital-elevation-model/copernicus#Elevation). Land covers are from FAO (https://www.fao.org/land-water/land/land-governance/land-resources-planning-toolbox/category/details/en/c/1036355/, https://data.apps.fao.org/catalog//iso/7f4f5ce4-9a3e-406f-bae6-efe63867329a) and ESA Climate Change Initiative (CCI) (https://climate.esa.int/en/projects/land-cover/, https://maps.elie.ucl.ac.be/CCI/viewer/index.php). Recent past (2000-2019) and future (2041-2060) climate data (precipitation, temperature) were downloaded from WorldClim 2.1 database (https://www.worldclim.org).

The harmonized grid maps of the soil abiotic and climate-classified database, grouped into thematic classes and reported in Supplementary Table 23, will be made publicly available through a repository to be specified upon acceptance/publication (URL to be provided).

Code availability

Data processing and analysis were conducted in QGIS Desktop (version 3.40.12) and MATLAB (release R2024b, update 5).

References

1. Cramer, W., Guiot, J. & Marini, K. *Risks Associated to Climate and Environmental Changes in the Mediterranean Region. A Preliminary Assessment by the MedECC Network Science-Policy Interface - 2019*. (MedECC, 2019).
2. IPCC. *Climate Change 2022 – Impacts, Adaptation and Vulnerability: Working Group II Contribution to the Sixth Assessment Report of the Intergovernmental Panel on Climate Change.* (Cambridge University Press, 2022).
3. Aurelle, D. *et al.* Biodiversity, climate change, and adaptation in the Mediterranean. *Ecosphere* **13**, e3915 (2022).
4. Petropoulos, S. A., Karkanis, A., Martins, N. & Ferreira, I. C. F. R. Edible halophytes of the Mediterranean basin: potential candidates for novel food products. *Trends Food Sci. Technol.* **74**, 69–84 (2018).
5. Grigoriadou, K., Krigas, N., Lazari, D. & Maloupa, E. Chapter 4 - Sustainable use of mediterranean medicinal-aromatic plants. in *Feed Additives* (eds. Florou-Paneri, P., Christak, E. & Giannenas, I.) 57–74 (Academic Press, 2020). doi:10.1016/B978-0-12-814700-9.00004-2.
6. Hunter, D. *et al.* The potential of neglected and underutilized species for improving diets and nutrition. *Planta* **250**, 709–729 (2019).
7. Ben Hamed, K. *et al.* Halophyte based Mediterranean agriculture in the contexts of food insecurity and global climate change. *Environ. Exp. Bot.* **191**, 104601 (2021).
8. Navarro-Torre, S. *et al.* Sustainable agricultural management of saline soils in arid and semi-arid Mediterranean regions through halophytes, microbial and soil-based technologies. *Environ. Exp. Bot.* **212**, 105397 (2023).
9. Zenobi, S. *et al.* Crithmum maritimum L . Biomass Production in Mediterranean Environment. *Agronomy* **12**, 926 (2022).

10. Kraouia, M. *et al.* Sea Fennel (Crithmum maritimum L.) as an Emerging Crop for the Manufacturing of Innovative Foods and Nutraceuticals. *Molecules* **28**, 4741 (2023).

11. Slot, L. E. & Fort, F. Drivers of Adoption of Sustainable Prickly Pear (Opuntia ficus-indica) Innovations and Conservation Agriculture by Smallholder Farmers in Morocco. *Agronomy* **14**, 3014 (2024).

12. Cattaneo, A. *et al.* Worldwide delineation of multi-tier city – regions. *Nature Cities* **1**, 469–479 (2024).

13. Ferreira, C. S. S., Seifollahi-Aghmiuni, S., Destouni, G., Ghajarnia, N. & Kalantari, Z. Soil degradation in the European Mediterranean region: Processes, status and consequences. *Science of the Total Environment* **805**, 150106 (2022).

14. Tramblay, Y., Llasat, M. C., Randin, C. & Coppola, E. Climate change impacts on water resources in the Mediterranean. *Reg. Environ. Change* **20**, 4–6 (2020).

15. Munns, R. & Gilliham, M. Salinity tolerance of crops - what is the cost? *New Phytologist* **208**, 668–673 (2015).

16. Stavi, I., Thevs, N. & Priori, S. Soil Salinity and Sodicity in Drylands: A Review of Causes, Effects, Monitoring, and Restoration Measures. *Front. Environ. Sci.* **9**, 712831 (2021).

17. Thaker, P. N., Brahmbhatt, N. & Shah, K. A review: impact of soil salinity on ecological, agricultural and socioeconomic concerns. *Int. J. Adv. Res. (Indore).* **9**, 979–986 (2020).

18. Fick, S. E. & Hijmans, R. J. WorldClim 2: new 1-km spatial resolution climate surfaces for global land areas. *International Journal of Climatology* **37**, 4302–4315 (2017).

19. Harris, I., Osborn, T. J., Jones, P. & Lister, D. Version 4 of the CRU TS monthly high-resolution gridded multivariate climate dataset. *Sci. Data* **7**, 1–18 (2020).

20. Aschonitis, V., Bilias, F. & Marques, K. *MS20. Soil Quality Classification Thresholds/Baselines". Report of the GOV4ALL Project 'Governance and Business Models for Living Labs: Rural Regeneration Hubs for Tackling Soil Health Challenges in the Mediterranean Region'*. (2025).

21. Dexter, A. R. Soil physical quality Part I . Theory, effects of soil texture, density, and organic matter, and effects on root growth. *Geoderma* **120**, 201–214 (2004).

22. Dexter, A. R. Soil physical quality : Part II. Friability, tillage, tilth and hard-setting. *Geoderma* **120**, 215–225 (2004).

23. Dexter, A. R. Soil physical quality Part III : Unsaturated hydraulic conductivity and general conclusions about S-theory. *Geoderma* **120**, 227–239 (2004).

24. Wösten, J. H. M., Lilly, A., Nemes, A. & Le Bas, C. Development and use of a database of hydraulic properties of European soils. *Geoderma* **90**, 169–185 (1999).

25. Hassink, J. The capacity of soils to preserve organic C and N by their association with clay and silt particles. *Plant Soil* **191**, 77–87 (1997).

26. Georgiou, K. *et al.* Global stocks and capacity of mineral-associated soil organic carbon. *Nat. Commun.* **13**, 3797 (2022).

27. Six, J., Doetterl, S., Laub, M., Müller, C. R. & Broek, M. Van De. The six rights of how and when to test for soil C saturation. *SOIL* **10**, 275–279 (2024).

28. Breure, T. S. *et al.* Revisiting the soil carbon saturation concept to inform a risk index in European agricultural soils. *Nat. Commun.* **16**, 2538 (2025).

29. Hargreaves, G. H. & Samani, Z. A. Estimating potential evapotranspiration. *Journal of the Irrigation and Drainage Division* **108**, 223–230 (1982).

30. Hargreaves, G. H. & Samani, Z. A. Reference crop evapotranspiration from ambient air temperature. in *American Society of Agricultural Engineers* 12 (1985).

31. Aschonitis, V. *et al.* High-resolution global grids of revised Priestley – Taylor and Hargreaves – Samani coefficients for assessing ASCE-standardized reference crop evapotranspiration and solar radiation. *Earth Syst. Sci. Data* **9**, 615–638 (2017).

32. Allen, R. G. *et al. The ASCE Standardized Reference Evapotranspiration Equation*. (American Society of Civil Engineers, Reston, Virginia, 20191-4400, 2005).

33. Allen, R. G., Pereira, L. S., Raes, D. & Smith, M. Crop Evapotranspiration: Guidelines for computing crop water requirements. Irrigation and Drainage Paper 56. *Food and Agriculture Organization of the United Nations* (1998).

34. Weiß, M. & Menzel, L. A global comparison of four potential evapotranspiration equations and their relevance to stream flow modelling in semi-arid environments. *Advances in Geosciences* **18**, 15–23 (2008).

35. UNEP. *World Atlas of Desertification*. (United Nations Environment Program, London, 1997).

36. Cherlet, M. *et al. World Atlas of Desertification Rethinking Land Degradation and Sustainable Land Management*. (Publication Office of the European Union, Luxembourg, 2018). doi:https://doi.org/10.2760/9205.

37. FAO. *Guidelines for Soil Description*. (FOOD AND AGRICULTURE ORGANIZATION OF THE UNITED NATIONS, Rome, 2006).

38. USDA-NRCS. *Soil Survey Manual: Agriculture Handbook No. 18*. (2017).

39. Ivushkin, K. *et al.* Remote Sensing of Environment Global mapping of soil salinity change. *Remote Sens. Environ.* **231**, 111260 (2019).

40. Soil Survey Staff. *Soil Survey Field and Laboratory Methods Manual. Soil Survey Investigations Report No. 51, Version 2.0.* (U.S. Department of Agriculture, Natural Resources Conservation Service, 2014).

41. Hazelton, P. & Murphy, B. *Interpreting Soil Test Results: What Do All The Numbers Mean?* (CSIRO Publishing, Melbourne, 2007).

42. Gamo, M., Shinoda, M. & Maeda, T. Classification of arid lands, including soil degradation and irrigated areas, based on vegetation and aridity indices. *International Journal of Remote Sensing ISSN:* **34**, 6701–6722 (2013).

43. Zarei, A. R., Shabani, A. & Mahmoudi, M. R. Comparison of the climate indices based on the relationship between yield loss of rain-fed winter wheat and changes of climate indices using GEE model. *Science of the Total Environment* **661**, 711–722 (2019).

44. Soil Survey Staff. *Field Book for Describing and Sampling Soils, Version 4.0.* (USDA, Natural Resources Conservation Service. U.S. Government Printing Office, 2024).

45. Körner, C. The use of 'altitude' in ecological research. *Trends Ecol. Evol.* **22**, 569–574 (2007).

46. Hijmans, R. J., Cameron, S. E., Parra, J. L., Jones, G. & Jarvis, A. Very high resolution interpolated climate surfaces for global land areas. *International Journal of Climatology* **25**, 1965–1978 (2005).

47. Demertzi, K., Papamichail, D., Aschonitis, V. & Miliaresis, G. Hydroclimatic analysis of Greece using multi-parametric clustering of monthly precipitation and reference crop evapotranspiration. *European Water* **55**, 141–155 (2016).

48. Rubin, J. Optimal Classification into Groups: An Approach for Solving the Taxonomy Problem. *J. Theor. Biol.* **15**, 103–144 (1967).

49. James, G., Witten, D., Hastie, T. & Tibshirani, R. *An Introduction to Statistical Learning with Applications in R*. (Springer, 2021).

Acknowledgements

The research presented here was conducted in the framework of the project VENUS - "ConVErting marginal lands of the Mediterranean basin into productive and sustainable agroecosystems using low water demanding Neglected and Underutilized Species" funded by the PRIMA programme (Grant Agreement No. 2312) supported by the European Union's Horizon 2020 research and innovation programme.

Contributions

C.D.L., L.T., M.C., and S.D. conceived and designed the study. L.T., C.D.L., wrote the original manuscript. C.D.L. and M.C. were responsible for data collection, processing, and analysis. M.C., C.D.L., L.T., and S.D. interpreted the findings. T.H., F.J., M.L.K., and V.A. contributed to the evaluation, interpretation, and discussion of the results. V.A., L.T., and T.H. secured funding for the project. All the authors revised and approved the final manuscript.

Corresponding authors

Correspondence to: Luigi Tosi, Cristina Da Lio

Ethics declarations

Competing interests

The authors declare no competing interests

Supplementary Files

This is a list of supplementary files associated with this preprint. Click to download.

- SupplInfoMappingmarginallands.docx